

Dynamics of isotropic and drifting plasmas in the vicinity and within two-dimensional finite dust clusters

G V Miloshevsky and A Hassanein

Center for Materials under Extreme Environment, School of Nuclear Engineering, Purdue University,
400 Central Drive, West Lafayette, IN 47907-2017, USA

E-mail: gennady@purdue.edu

Received 22 September 2011, in final form 13 February 2012


Published 16 March 2012

Online at stacks.iop.org/PPCF/54/045006

Abstract

2D finite dust clusters are systems of small number of charged grains immersed in the plasma. The particle-in-cell (PIC) simulations are used to study the plasma structure, potential field and distributions of ion, electron and charge density within a dust cluster consisting of 19 grains in the absence and presence of a directed ion flow. In the isotropic plasma, an energetically stable configuration of this 2D finite dust cluster is found with overlapping ion clouds within the cluster's area. The supersonic ion flow transforms the common potential well to a shallow oval basin with the formation of an elongated potential hill behind the dust cluster. The common wake region with strong ion focusing is developed with the number density of ions significantly exceeding that in bulk plasma and within a cluster. The region within a dust cluster remains highly depleted of electrons even at supersonic ion flows. The charge on one of grains switches to a positive value. The kinetic-level PIC results provide insights into development of instabilities that can initiate the cluster reorganization, disordering and melting.

(Some figures may appear in colour only in the online journal)

 Online supplementary data available from stacks.iop.org/PPCF/54/045006/mmedia

1. Introduction

Complex plasmas consist of dust grains immersed in the background of gaseous plasma of electrons, ions and neutral atoms [1, 2]. Dusty plasma can be strongly coupled, i.e. the interaction energy between the dust grains can exceed their kinetic energy [3]. The dust–plasma crystal formation is one of the most striking examples of dust self-organization when micrometer-sized grains form regular arrays exhibiting various lattice-like structures [4–7]. They can range widely in size, shape, order, symmetry and can represent different forms of self-organization such as clouds and voids, 2D and 3D crystalline lattices, strings and agglomerates [2, 3]. The formation of dust clusters consisting of a small number of grains was also observed in experiments with an external confining potential [8, 9]. The formation of boundary-free (unconfined) dust cluster was recently reported in experiments performed under microgravity conditions [10]. These finite dust clusters are similar to finite Coulomb clusters found in colloidal suspensions with macroscopic particles [11, 12], and electrons on a liquid helium surface [13]. However, the crucial

difference is that the charges on dust grains fluctuate according to the plasma conditions. Since the number of grains is small, the interactions between the grains are non-collective [14]. One of the fundamental questions is the understanding of the plasma–grain as well as the inter-grain interactions in finite dust clusters. The basic processes such as grain charging, electric potential distribution around and within a small dust cluster, inter-grain repulsion or attraction, electron and ion number density distributions, charge density distribution are of direct relevance.

The dynamic and thermodynamic behavior of finite clusters of charged grains were investigated both theoretically and experimentally [14, 15]. Theoretical analysis and modeling was focused on structural configurations [16, 17] and normal modes [18–21] of 2D finite dust clusters. It was predicted theoretically that the normal mode with the lowest excitation energy in 2D finite clusters is an inter-shell rotation of two neighboring concentric rings of the cluster [18]. Experimental studies treated cluster melting using direct laser heating of the grains [22] and cluster excitation by placing a single grain behind a dust cluster in the ion wakefield [23, 24].

The attraction due to the ion focus induces unstable oscillations leading to melting of 2D finite dust clusters. The zigzag transition from 1D linear chain of grains to 2D dust structures was also reported [25]. In the other experiment, two opposing laser beams were used to excite the inter-shell rotation of grains in the $N = 19$ cluster with two neighboring shells rotating with respect to each other [26]. The inter-shell rotations were observed in agreement with the earlier theoretical predictions [18]. All this theoretical and experimental work was focused on the structural and dynamical properties of 2D finite clusters. We should note that grain charging, kinetics and dynamics of plasma ions and electrons interacting with negatively charged grains, plasma charge distributions during melting transitions are microscopic plasma-driven mechanisms underlying those macroscopic processes.

The quantitative description of finite dust systems remains a challenge for both theory and simulation [27]. It is not possible to interpret the effects of collective charging in the presence of many grains by applying the information about the charging of an isolated grain. The most important issue is that a separation of charging and shielding is not possible in a many-grain plasma system since shielding is affected by charging and vice versa. The electrostatic energy between the two dust grains surrounded by Debye plasma spheres (dressed grains) should include four terms describing the interaction between two dust grains, two Debye plasma spheres and grain–Debye sphere cross-interactions [28]. At certain inter-grain separations, it was predicted that an attractive part can appear in the interaction potential between two dressed grains [28]. In the presence of supersonic ion flows, the influence of the ion drift on charging and screening of grains is significant. The charge state and interactions between grains can be qualitatively changed by the ion flow. The symmetric cloud of ions around each grain is deflected downstream due to the ion flow. The concept of the wakefield was introduced by Nambu *et al* [29]. It was demonstrated that an oscillatory wake potential arising from the collective interactions between the dust grains and acoustic waves [30] can cause attraction between grains. The ions can be focused in the negative potential region of the wakefield attracting other negatively charged dust grains [31]. The common wake, a perturbed region of ion density, can be formed behind a dust cluster due to the collective effect of cluster's grains. The formation of wakefields was mainly studied for one or two grains [32–38]. These results can provide only rough insights into understanding the complex interplay between charging and screening in dust clusters formed by many grains. In the presence of dust clusters, the wakefield attraction observed for a linear chain of grains levitating in the sheath can be modified. It was shown that the wakefields merge when the distance between the two grains becomes small [34, 35].

In this work, we investigate first the stationary plasma structure, potential field and distribution of ions, electrons, and charge density within a 2D dust cluster built from 19 grains in the absence of a directed ion flow. An energetically stable configuration of this finite cluster is found with certain inter-grain separations in isotropic plasma. Then, we expose this dust cluster to a subsonic and supersonic ion flow. The ion

flow speeds and other microscopic plasma characteristics can be manipulated in experiments by varying the discharge plasma power [24]. The results are reported on the effect of a directed ion flow on the structure of ion clouds within a dust cluster, the formation and structure of the wake potential and charge behind a dust cluster, the number distribution of plasma ions and electrons and the charge state of dust grains. The results provide key insights into the atomistic processes underlining large charge variations potentially triggering instability in a 2D finite dust cluster due to a directed ion flow. Our work is more relevant to plasmas under microgravity conditions and boundary-free dust clusters such as the experimental set-up with a long glass Π -tube used in recent experiments to observe a boundary-free dust cluster [10].

2. Numerical method

We have developed a 2D particle-in-cell (PIC) code to model dust clusters in plasmas. The code is written in mixed Fortran-90/C++ language. The technical implementation of our 2D PIC scheme is conventional to PIC plasma models described in classical textbooks [39, 40]. We briefly summarize the fundamental steps of the PIC model: (1) the electron and ion macro-particles are assigned Cartesian coordinates and velocities within a 2D computational domain; (2) the spatial grid over the computational domain is created; (3) the charge of electron and ion macro-particles in each cell is distributed among the nearest grid points; (4) the charge density on the grid is then used as the source in Poisson's equation which is solved numerically producing the electrostatic potential at each grid point; (5) the electric field is evaluated on the grid; (6) the force due to the electric field is interpolated from the discrete grid to the plasma macro-particle locations; (7) plasma macro-particle velocities and positions are advanced on the time step. This PIC approach smears out each point charge of macro-particles into a finite-sized charge distribution on the grid [40]. Thus the strong short-range interaction of charged point macro-particles is eliminated. Because of this procedure the PIC method describes correctly only long-range electrostatic forces. Additional features implemented in our PIC model are accurate resolution of (1) finite size of small dust grains and (2) trajectories of plasma macro-particles close to dust grains with treatment of short-range forces using direct plasma particle–grain force calculations (molecular dynamics (MD) method).

For plasma simulations, the splitting of the inter-particle force into the short-range and long-range components (Particle–Particle Particle–Mesh (P^3M) algorithm) was originally introduced by Hockney and Eastwood [39]. The idea of the P^3M method is to compute the total short-range force on plasma particle i , which is non-zero for particle separations less than some cut-off distance, by direct particle–particle (PP) pair force summation, while the long-range force is approximated by the particle–mesh (PM) force calculation [39]. The P^3M technique was adapted to model dusty plasmas [41]. Both the short-range and long-range interactions between dust grains 'dressed' by the plasma were accurately represented. The plasma was modeled implicitly using the plasma dielectric

function. This approach was implemented in the Dynamically Shielded Dust (DSD) code with technical details described in separate steps with bullets [41]. The DSD technique was used by us to model the direct plasma–dust interactions in the vicinity of dust grains. The dust grains are usually much smaller than the PIC mesh size. It was demonstrated that the PIC scheme does not treat correctly the short-range interactions within the length of one–two cells [41–43]. With decreasing separation between two charged particles, the interaction force decreases to zero instead of increasing [41]. The short-range force on plasma macro-particles in the vicinity of a dust grain should be calculated directly. Therefore, the cell confining a dust grain with plasma macro-particles and the nearest neighbor cells with macro-particles (figures 4 and 5 in [41]) are treated using the direct PP scheme. Our implementation of the P³M technique follows that described in detail in [41]: (1) assign the charges to the grid points using the linear weighting; (2) solve Poisson’s equation on the mesh to determine the PIC potential and force; (3) calculate the direct PP force due to the short-range interactions between dust grains and plasma macro-particles and (4) update the positions and velocities of plasma macro-particles due to the resulting PIC and direct PP force. This is a classical P³M scheme [39] where the direct PP method is used to find the short-range contribution to the force on plasma macro-particles and the PM method is used to find the PIC force contribution. The reduced time step is used for plasma macro-particles in the vicinity of dust grains to accurately resolve their trajectories [43]. This implementation was needed to correctly determine the charge and floating potential on small dust grains. A different implementation of the PIC/MD method in terms of the electric field is briefly discussed in [38, 42] without providing technical detail. In this scheme, the total electric field acting on the plasma electrons and ions is corrected by subtracting the PIC electric field due to a dust grain and adding the MD electric field originating from a dust grain. Insufficient details are provided in this model on how the PIC contribution due to a dust grain is separately calculated on the grid. The PIC/MD descriptions in [38, 42] closely resemble each other without referring to each other or any previous PIC/MD work. The multi-frontal massively parallel solver, MUMPS [44], is used to solve the Poisson equation at each time step. It is an accurate direct method based on lower and upper matrix factorization. The MUMPS solver utilizes the MPI library and uses the BLAS, BLACS and ScaLAPACK libraries.

The set-up of the simulation system is illustrated in figure 1. The computational domain represents a 2D plane with X and Y lengths 0.01 m. A grid with spacing $50\ \mu\text{m}$ (200×200 cells) is used. On the domain’s boundaries, the electric potential is assumed to be fixed corresponding to that of unperturbed bulk plasma, ~ 0 V. The electron number density and temperature are $N_e = 10^{15}\ \text{m}^{-3}$ and $T_e = 3\ \text{eV}$ resulting in an electron Debye length of $\lambda_{De} \approx 407.2\ \mu\text{m}$. The number of electron Debye lengths per domain length is ~ 25 . The electron plasma frequency is $\omega_e \sim 1.8 \times 10^9\ \text{s}^{-1}$. The ion number density N_i is the same as that of electrons. The ion temperature is $T_i = 0.03\ \text{eV}$ yielding $T_i/T_e = 0.01$.

The ratio of ion to electron mass was set to 200. The computation time is intractably large if a physical mass ratio is

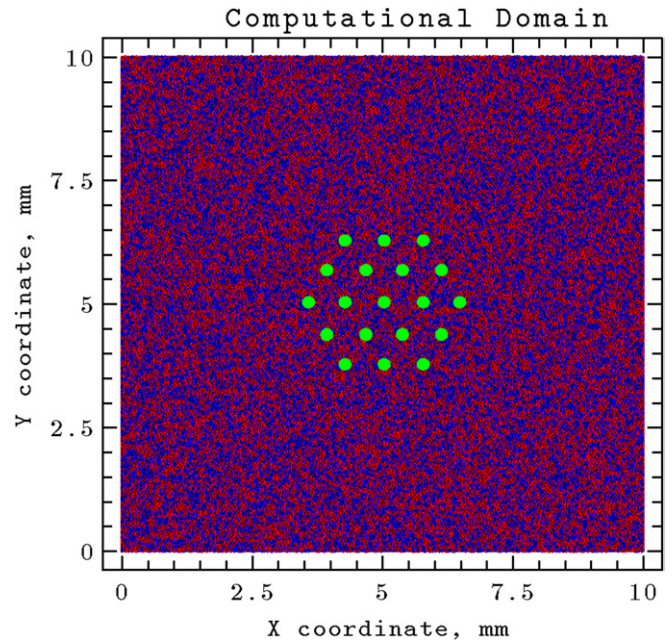


Figure 1. Computational domain used in PIC simulations of a dust cluster with 19 grains shown as green spheres and immersed in the isotropic plasma. There are $\sim 10^6$ ions (red points) and $\sim 10^6$ electrons (blue points). The grains with radius of $5\ \mu\text{m}$ are magnified by 25 times to make them visible.

utilized in the code. It was recognized early by Hockney and Eastwood [39] that the PIC results are valid if a sufficiently large ion/electron mass ratio is used. A large body of later work shows that the ratio ~ 120 allows for simulating a realistic process giving credible results [36–38, 45]. The effect of different mass ratios on the floating potential was investigated in [45] concluding that it is not critical to have completely realistic mass ratio values in the PIC simulations. We have specifically performed the PIC probe simulations with the physical proton/electron ratio ~ 1896 for some particular cases, not observing the crucial change in the behavior of our plasma–dust system. The ion Debye length is $\lambda_{Di} \approx 40.7\ \mu\text{m}$. The total Debye length is $\lambda_D \approx 40.5\ \mu\text{m}$. The plasma is modeled as collisionless since the number of plasma particles in a sphere with radius equal to the Debye length is much larger than one, $N_D \sim 33$. The collisions and short-range interactions can be neglected. Long-range particle–particle interactions are mediated by the electric field computed at the points of a discrete grid. Thermal velocities of macro-electrons and macro-ions are $v_e \sim 7.3 \times 10^5\ \text{m s}^{-1}$ and $v_i \sim 5.1 \times 10^3\ \text{m s}^{-1}$, respectively. The ion acoustic velocity is $v_s \sim 5.2 \times 10^4\ \text{m s}^{-1}$. The time step is $\sim 10\ \text{fs}$, that is $\sim 0.02/\omega_e$. The total number of simulation macro-electrons and macro-ions initially placed within the computational domain is $\sim 2 \times 10^6$. Each macro-particle represents one real plasma particle. The number of macro-particles per cell is ~ 50 , that is even larger compared with that in the Debye sphere N_D . This ensures that spurious oscillations due to the relatively small number of simulation particles are avoided. The plasma at the boundaries is modeled as unperturbed. In our PIC model, plasma macro-particles are free to leave the computational domain through any boundary, and new plasma macro-particles are injected from

the boundaries. The injecting boundaries maintain the flux of macro-particles with the Maxwellian velocity distributions. The modeled region effectively represents an infinite plasma system of large spatial extent. The potential energy U at time t_n is the sum of a product of the charge density ρ_{ij} and the potential ϕ_{ij} over all grid points [40]

$$U(t_n) = \sum_{i,j}^{I,J} \rho_{ij}(t_n) \phi_{ij}(t_n) \Delta s_{ij},$$

where Δs_{ij} is the area of ij cell, I and J are the number of grid points in the X and Y directions, respectively. The kinetic energy K at time t_n is given by the sum of the kinetic energies of plasma ions and electrons [39, 40]

$$K(t_n) = \frac{1}{2} \sum_{k=1}^N m_k \frac{v_k^2(t_{n-1/2}) + v_k^2(t_{n+1/2})}{2},$$

where N is the total number of plasma macro-particles, m_k and v_k are the mass and velocity of k th macro-particle. The total energy at time t_n is then the sum of the potential and kinetic energies. In the case of subsonic or supersonic ion flow, the ions have the drift velocity, v_d , along the X axis (the Mach number $M = v_d/v_s$). The dust grains are considered as motionless. The mass of grains is many orders of magnitude larger than the mass of plasma ions. Therefore, the time scales of plasma ions are on the order of microseconds while the dust grains move on the order of milliseconds. Structural changes in clusters usually occur on timescales of the order of seconds. The dust grains with radius of $5 \mu\text{m}$ were initially preconfigured into a symmetric dust cluster with 19 grains. The distance between grains was symmetrically varied. The dust cluster was placed in the center of the computational domain. Grains were treated as insulating particles. Our focus is on the dynamics of electrons and ions and non-linear plasma effects in the presence of a stationary dust cluster. The charge and potential on grains was constructed by absorbing the plasma macro-particles until they start to fluctuate around an average value. The simulations were run up to $\sim 5 \mu\text{s}$ (~ 100 ion plasma periods).

3. Results and discussion

2D stationary distributions of electric potential, charge, number of ions and electrons within a dust cluster composed of 19 insulating grains and immersed in isotropic plasma are reported in this section. The effects of subsonic and supersonic ion flows on the microscopic structure of the plasma and formation of a wake behind this dust cluster are also presented.

3.1. Plasma structure within/behind a dust cluster

In isotropic plasma, the inter-grain separation in a preconfigured dust cluster with 19 grains (figure 1) was scaled around an electron Debye length to identify the energetically favorable configurations that minimize the total energy of the plasma-grain system. It is found that dust clusters with inter-grain separations in the range

$\sim 0.6\lambda_{De} - 0.8\lambda_{De}$ are energetically more favorable compared with other configurations with smaller or larger inter-grain distances [46]. At large inter-grain separations $\geq \lambda_{De}$, the isolated clouds of ions surrounding the dust grains are formed. At inter-grain separation $\sim 0.6\lambda_{De}$, the ionic clouds overlap forming a common cloud of ions within the entire area of a dust cluster (figure 2(a)). We have explained that a self-consistent state of a dust cluster is due to the kinetic effects of plasma ions and electrons [46]. This is a state in which the strong grain's repulsion is surmounted by the reduced charge and floating potential on grains, overlapped ion clouds and depleted electrons within a cluster. The PIC simulations of finite 2D dust clusters with 2, 3 and 7 grains were also carried out. For all of them the energetically favorable state was observed at certain inter-grain separations. However, the energy minimum was shifted to smaller inter-grain separations with decrease of the number of grains. For example, the dust cluster with 7 grains has demonstrated the energy minimum at inter-grain separations $\sim 230 \mu\text{m}$. For the dust cluster with three grains, the total energy has reached a minimum at inter-grain separations $\sim 100 \mu\text{m}$. For two dust grains, the energetically favorable state was found at $\sim 90 \mu\text{m}$. This intriguing possibility of self-organization of dust grains into clusters was originally predicted by Tsytovich and coworkers [47].

It was later proved theoretically for two dust grains that the ion shielding not only partially reduces the repulsion between grains, but there is attraction leading to the self-confinement [28, 48, 49]. The MD simulations were also performed reporting the boundary-free dust clusters [50]. It was shown theoretically that a stable 2D grain cluster can exist in plasmas without external confinement [51]. Moreover, a self-confined dust cluster was indeed observed in experiments under microgravity conditions [10]. This theoretical, computational and experimental evidence on self-confined dust clusters strongly supports our PIC results. The subsonic ion flow (figure 2(b)) shifts the common ion cloud toward the right boundary of the cluster. The cluster's area becomes ion depleted. The ions are concentrated on the most peripheral grains. The supersonic ion flow (figures 2(c) and (d)) shifts further the common ion cloud positioning it behind a dust cluster. At high ion flow speeds (figure 2(d)), the strips of ions are seen between rows of grains within a dust cluster with the well developed ion focus in the downstream direction. The physical explanation is due to the fact that ions are scattered into the wake behind a dust cluster contributing to the ion focus (region of enhanced ion density). Supplementary movies show the dynamics of plasma ions and electrons within and behind a dust cluster for isotropic (online supplementary data) and drifting (online supplementary data) plasma conditions.

3.2. Topology of potential field within/behind a dust cluster

The potential map within a dust cluster is shown in figure 3 for the time moment $t \sim 5 \mu\text{s}$. With no ion flow (an isotropic plasma), the dust cluster composed of 19 grains is trapped in a common potential well (figure 3(a)). This self-confining potential well is nearly spherically symmetric. The

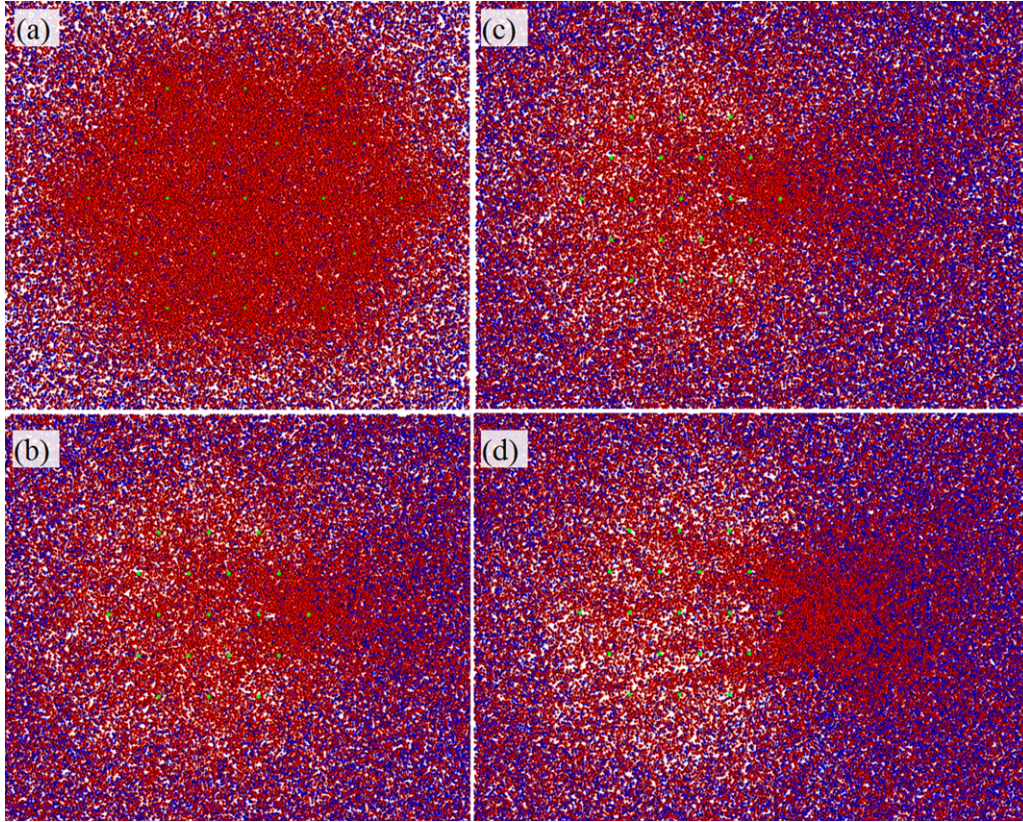


Figure 2. The distribution of ions (red dots) and electrons (blue dots) within a dust cluster composed of 19 grains with averaged inter-grain separations $\sim 0.6\lambda_{De}$ at time $\sim 5\mu s$. Dust grains are shown as small green spheres. The Mach number is (a) $M = 0$, (b) $M = 0.8$, (c) $M = 1.2$ and (d) $M = 1.4$. These snapshots are taken from the movies available at online supplementary data.

topology of the common potential well shows local potential wells separated by potential barriers. These isolated wells correspond to negatively charged grains. Since each grain's charge fluctuates, the landscape of potential wells and barriers (their depths and heights) is non-uniform. Some of the wells near the center of a dust cluster are deeper than others close to cluster's periphery. It is seen that the ion flow modifies the common potential well even in the direction perpendicular to the flow (figure 3(b)). Its depth increases by $\sim 2.4 V$. A complex non-uniform relief of the bottom transforms to an oval deep basin with rather steep slope near the right-hand side edge of the cluster. At supersonic ion speeds with $M \sim 1.4$ (figure 3(c)), the potential hill is formed behind the dust cluster. The depth of the common potential well within a dust cluster further decreases. At higher ion velocities (figure 3(d)), the potential hill grows with elongation in the direction of the ion flow. The common potential well becomes even more shallow and deformed. The oscillatory behavior of the potential behind a cluster cannot be observed due to a limited X length of the computational domain. The effects of the ion flow speed on the depth of the common potential well were also analyzed using the cut-off of the potential across the dust cluster at $Y = 5$ mm (results are not shown).

3.3. Number density of ions within/behind a dust cluster

The maps of the ion density are shown in figure 4 for four values of the speed of the ion flow at time $5\mu s$. The ion

density is normalized to the background ion density. It is seen that in the isotropic plasma with $M = 0$ (figure 4(a)), the number density of ions is much higher within the dust cluster (~ 12 times) compared with the bulk plasma. The ions are concentrated in the close vicinity of the dust grains, especially around the central grain and a nearby concentric shell formed by six grains. The ionic clouds overlap forming a common cloud of ions within the dust cluster. The number density of ions is slightly decreased on the peripheral shell of grains, and then drops to the bulk value away from the cluster. The subsonic ion flow with $M = 0.6$ (figure 4(b)) considerably modifies the distribution of ions within a dust cluster. The dust grains are marked as small brown balls. An ion focus establishes near the location of a peripheral grain on the right-hand side of a dust cluster. The common cloud of ions is highly perturbed with the spatial spreading in the flow direction. The number density of ions in the focus is about two times less compared with that found in isotropic plasma (figure 4(a)). The flow of ions with supersonic speeds (figures 4(c) and (d)) shifts further the ion focusing.

The strong ion focus is formed at the distance of the order of ~ 0.25 – 0.5 mm behind the dust cluster. The number density of ions at the focus now exceeds that within the dust cluster. With increase in the Mach number of the ion flow (figure 4(d)), the area of ion distribution becomes larger expanding in the flow direction. Clear regions of low ion density are seen on each side of the ion wake focus. Since the inter-grain separation in the cluster $\sim 0.6\lambda_{De}$ is smaller

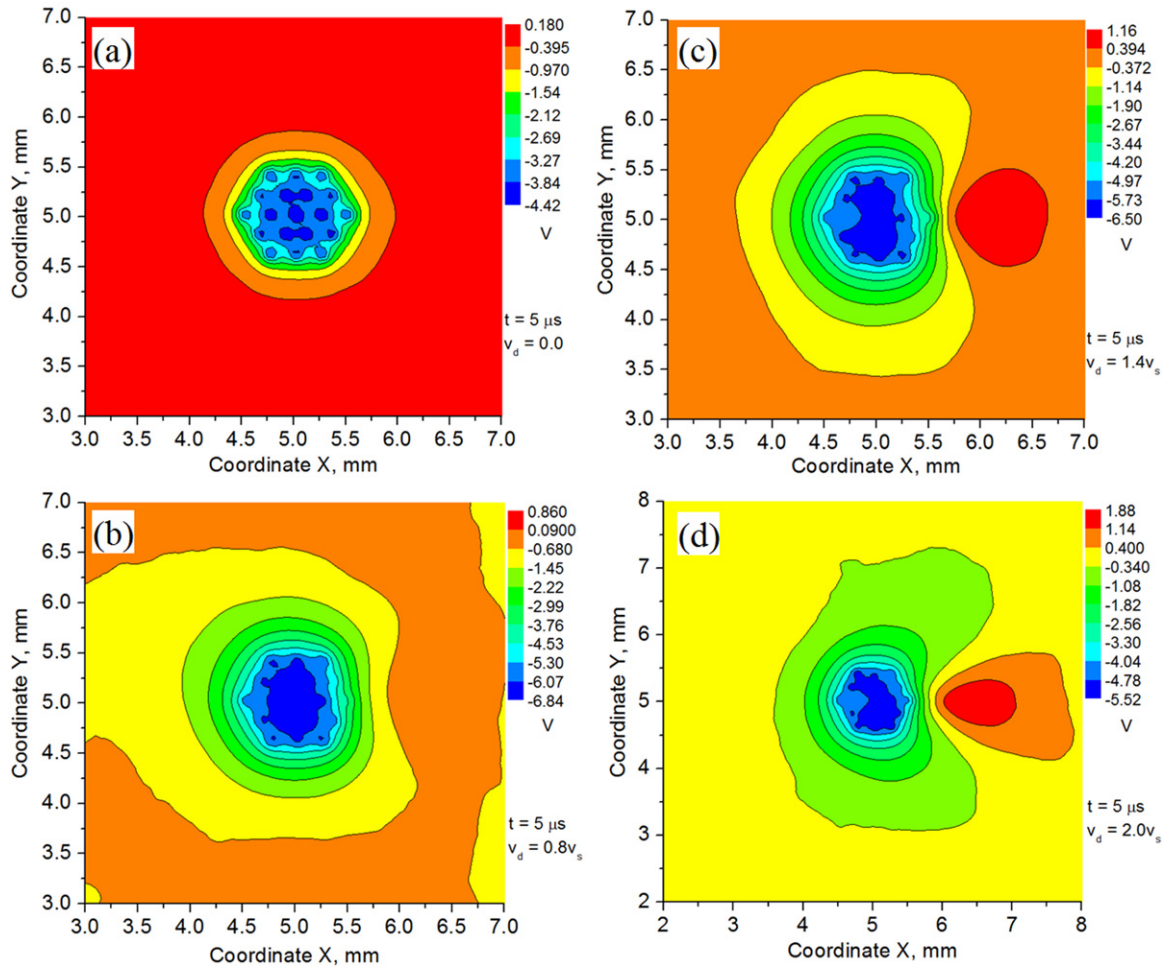


Figure 3. Contour plots of the plasma potential field within/behind a dust cluster with averaged inter-grain separations $\sim 0.6\lambda_{De}$ at time $\sim 5 \mu s$. The Mach number is (a) $M = 0$, (b) $M = 0.8$, (c) $M = 1.4$ and (d) $M = 2.0$, respectively.

than the electron Debye length, the observed effect of ion focusing is due to the collective contribution of all grains. It was clearly demonstrated for two grains aligned perpendicular to the ion flow that the ion wake focuses are well separated when the inter-grain distance is larger than the electron Debye length [34].

Our PIC modeling deals with collisionless ion trajectories. The effect of collisions on the charging process of an isolated dust grain was investigated using a Monte Carlo collision algorithm for operating conditions of interest to material processing [52]. For such conditions, the mean free path of ion-neutral charge-exchange collisions $\lambda_{in} = 1/N_n\sigma_{in}$ is of the order of λ_D . Here N_n is the number density of neutral gas and σ_{in} is the ion-neutral collision cross-section, typically $\sim 5 \times 10^{-15} \text{ cm}^2$ [53]. For dust grains with small radius, the charge-exchange collisions are found to be important even at low collision rates since ion orbits are destroyed by the dust grain within $\lambda_D \sim \lambda_{in}$ [52]. For our modeling plasma conditions, λ_{in} is estimated using characteristic lengths and times associated with complex plasmas [54] to be on the order of the size of dust clusters, $\lambda_{in} \sim 0.5\text{--}2 \text{ mm}$ depending on the value of N_n , much longer compared with λ_D . For various λ_{in} , the distribution of ions near a grain was also reported in the PIC simulations and calculated using the Debye approximation [55]. It is interesting to analyze these PIC

results for a rough estimate of the effect of missed collisions on the self-confinement of grains. With increasing collision frequency (reducing λ_{in}), it was observed that the PIC ion distribution evolves toward the Debye ion distribution [55]. For infinite λ_{in} (no collisions), it is found that PIC density of ions near the grain surface is about eleven times larger than bulk ion density. Although we used slightly different plasma conditions, our collisionless PIC results show that the ion density near grains is twelve times larger than that in the bulk plasma. However, both these collisionless PIC densities are about six times smaller compared with that calculated using the Debye distribution [55]. For $\lambda_{in} \sim 1000 \mu m$, the difference in PIC and Debye ion density near the grain surface reduces to 1.5 times. For $\lambda_{in} \sim 100 \mu m$, it is found that the profiles of PIC and Debye ion density coincide [55]. Thus, with account for charge-exchange collisions and trapped ions, we should expect even denser ion clouds. This means enhancement of the grain screening, reduction in the electrostatic repulsion between grains and enhancement of the self-confinement of grains.

3.4. Number density of electrons within/behind a dust cluster

The distribution of the normalized number density of electrons within/behind the dust cluster is shown in figure 5. In the case

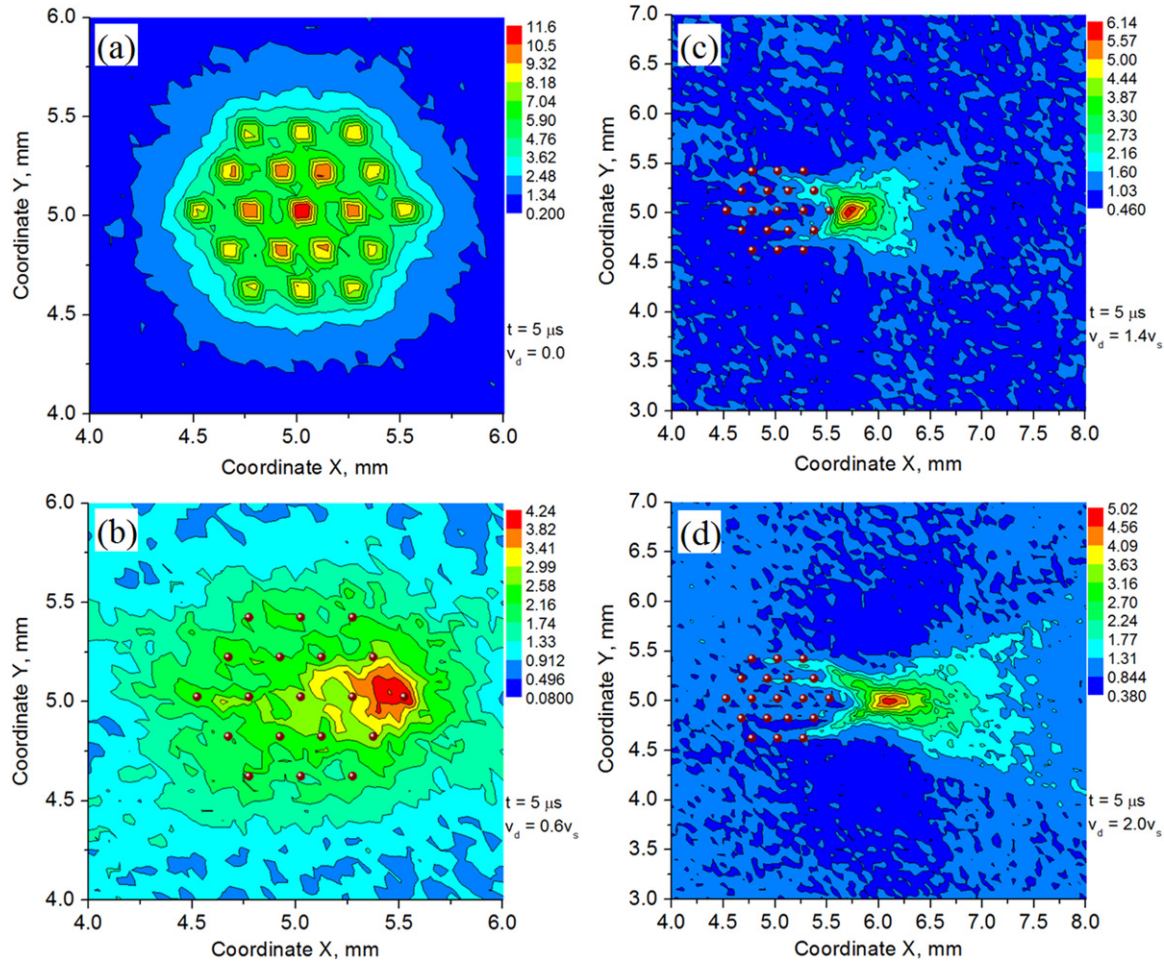


Figure 4. Contour plots of the number density of ions within/behind a dust cluster with averaged inter-grain separations $\sim 0.6\lambda_{De}$ at time $\sim 5 \mu s$. The Mach number is (a) $M = 0$, (b) $M = 0.6$, (c) $M = 1.4$ and (d) $M = 2.0$, respectively.

of isotropic plasma (figure 5(a)), the plasma region occupied by a dust cluster is highly depleted of electrons. The electron density is an order of magnitude less than the density of electrons in the bulk plasma.

The distribution of electron number density within a dust cluster is inhomogeneous with islands of slightly higher electron density. This electron-depleted region is deformed a bit by the subsonic ion flow with $M = 0.8$ (figure 5(b)). It takes an oval shape due to the expansion in the direction perpendicular to the ion flow. The ion flow with supersonic velocities (figures 5(c) and (d)) produces a cloud of electrons behind a dust cluster. The stripes of the number density of electrons are observed. The focusing of electrons, similar to that of ions shown in figures 4(c) and (d), is not seen. Since the average thermal velocities of electrons are greater than velocities of flowing ions, we suggest that the role of the observed electron cloud is to preserve the plasma quasineutrality in the ion wake focus.

3.5. Charge density within/behind a dust cluster

The distribution of the charge density per unit area is illustrated in figure 6. In the 2D system, the unit of charge is given as $C m^{-1}$. Therefore the charge density per unit area is expressed

in units $C m^{-3}$. The charge density was built by distributing the charge of each electron, ion and dust grain to the neighboring mesh points and then dividing by the cell's area. A complicated structure of the charge density around and within the dust cluster is observed. In the absence of ion flow (an isotropic plasma) (figure 6(a)), the charge density is positive between the grains within a dust cluster due to overlapped ionic clouds. At the location of dust grains, the charge density is highly negative because of a large negative charge accumulated on the grains. It is seen that the charge on seven grains forming a sub-cluster in the center of a dust cluster is more positive compared with the charge on other grains forming a peripheral shell. This is because the ion screening of those central grains is larger (see figure 4(a)). The subsonic ion flow with $M = 0.8$ modifies the distribution of the charge density. The ion focusing produced by upstream grains substantially reduces the negative charge on downstream grains. The charge density in the vicinity of the second grain (we call it grain no. 2) located in a central row composed of five grains becomes significantly more positive (figure 6(b)). More positive charge density is also acquired near the other grains of this central row, the grains located in the adjacent two rows as well as two intermediate grains in the most peripheral rows. The supersonic ion flow (figures 6(c) and (d)) switches the charge density to positive charge in the vicinity

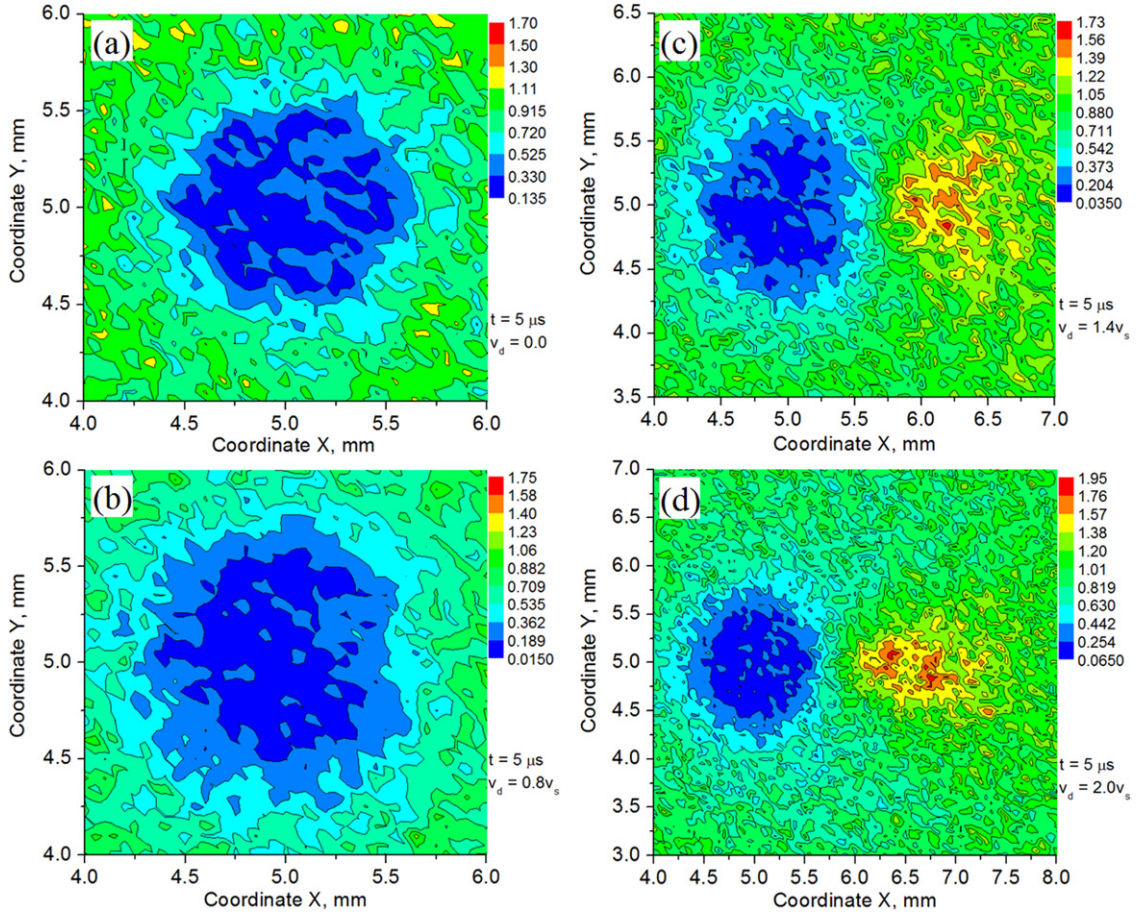


Figure 5. Contour plots of the number density of electrons within/behind a dust cluster with averaged inter-grain separations $\sim 0.6\lambda_{De}$ at time $\sim 5 \mu s$. The Mach number is (a) $M = 0$, (b) $M = 0.8$, (c) $M = 1.4$ and (d) $M = 2.0$, respectively.

of grain 2. The attraction of neighbor grains to the positive charge of grain 2 can substantially stabilize the dust cluster. The charge density near the central grain approaches zero (the charge density of unperturbed plasma). At $M = 1.4$ the region of positive charge density is formed behind the dust cluster (figure 6(c)). At higher Mach number $M = 2.0$, the charge distribution in the wake behind the dust cluster is modified. The region of positive charge is elongated by twice its length in the direction of the ion flow (figure 6(d)). Strips of positive charge density are seen within the dust cluster.

The time evolution of the charge on grain 2 is shown in figure 7(a) for various values of the Mach number. The charge on the grain is normalized per absolute value of the electron unit charge. Initially the grain acquires a large negative charge with its further relaxation to an equilibrium value. These sharp changes of charge indicate the grain charging and the build-up of a sheath. When the steady state is reached, the charge on dust grain fluctuates around an equilibrium value. With increase in the ion drift velocity, the value of grain's charge becomes less negative reaching positive values at supersonic ion speeds. The effect of Mach number on the value of charge on five dust grains located in a central row within a dust cluster is shown in figure 7(b).

The grains are numbered consecutively from left to right. Lines connecting grains are only for visual purpose. For each grain the charge was averaged over the last $2 \mu s$. At

subsonic ion flows with $M \leq 0.6$, the charge on grains is reminiscent of the symmetric zigzag line. The charge on grains becomes less negative with increasing Mach number (compare $M = 0.2$ and $M = 0.6$). The value of negative charge on grains 2 and 4 is decreased compared with that on grains 1, 3 and 5. The reason for this behavior is not fully understood. The ion flow is exactly directed along the lines of grains in the cluster. Presumably the effect is due to alternating focusing and defocusing of ions drifting with subsonic velocities across a lattice of grains. Further investigations are needed to clarify whether the orientation of the dust cluster relative to the ion flow direction has significant influence on this behavior. At $M = 0.8$, the zigzag symmetry is broken on grains 4 and 5. Less negative charge is acquired on grain 2. At a supersonic ion flow with $M = 1.2$, the charge on grain 2 becomes positive. With further increase in the Mach number, the charge variations on grains 1, 2 and 3 are relatively small. The charge fluctuates within ~ 1000 units on grains 4 and 5.

4. Conclusions

Our developed PIC model provides a fully kinetic description of complex plasmas with ability to treat self-consistently complex interplay between non-linear processes of grain

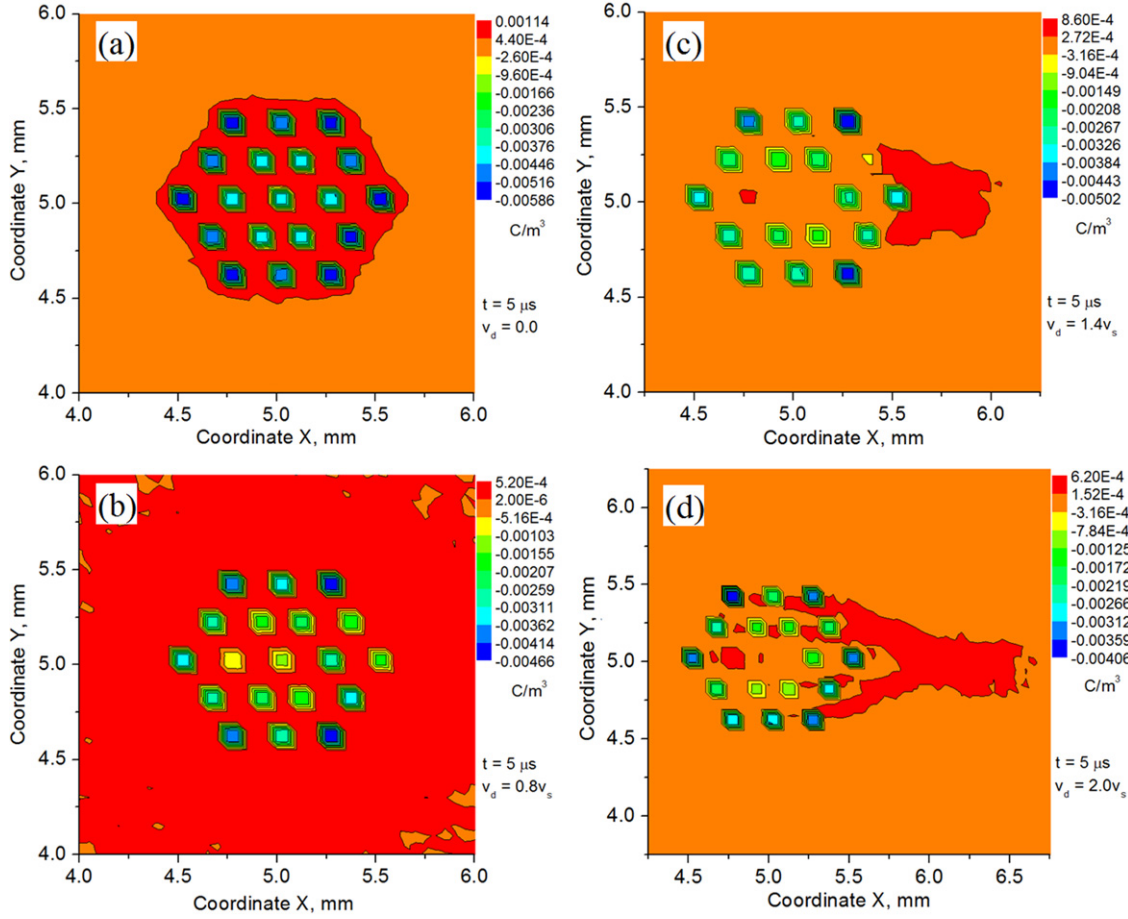


Figure 6. Contour plots of the charge density within/behind a dust cluster with averaged inter-grain separations $\sim 0.6\lambda_{De}$ at time $\sim 5 \mu s$. The Mach number is (a) $M = 0$, (b) $M = 0.8$, (c) $M = 1.4$ and (d) $M = 2.0$, respectively.

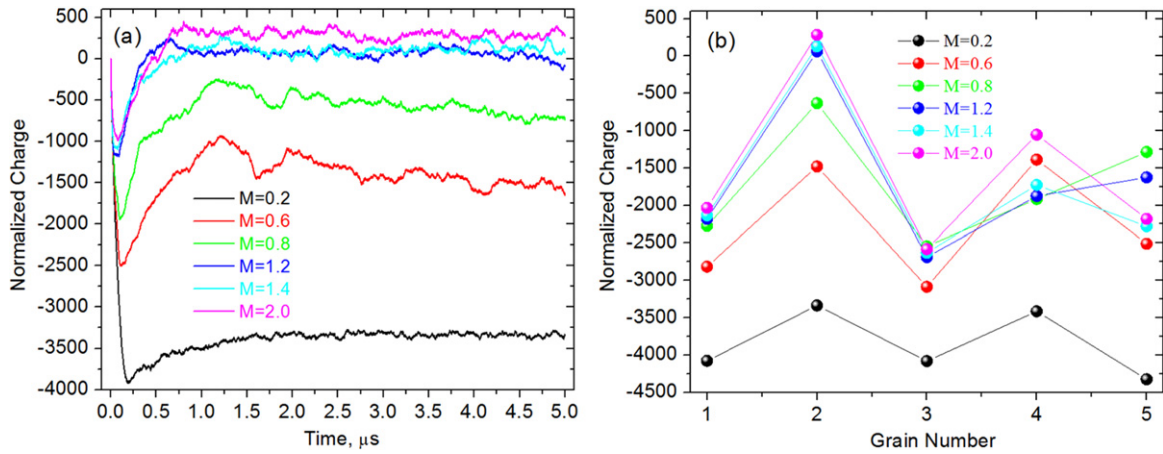


Figure 7. The time evolution of charge on grain 2 (a), and values of charge on five grains located in a central row within a dust cluster (b) for various values of the Mach number.

charging and screening, formation of sheaths around grains, discreteness of plasma particles and influence of plasma fluxes through grain surfaces on floating potentials. The microscopic structure of isotropic plasma within a stationary, preconfigured dust cluster composed of 19 grains is studied on ion timescales (microseconds). The influence of the ion drift with subsonic and supersonic speeds on the distribution of plasma ions and electrons, electric potential, grain charging and charge states of

grains within/behind this finite dust cluster is also investigated. We find that the ions affect the plasma shielding at the location of a dust cluster, the floating potential and the charge on grains. In the absence of a directed ion flow (an isotropic plasma), an energetically stable configuration of a dust cluster with inter-grain separation $\sim 0.6\lambda_{De}$ is found in which the ion clouds around individual grains overlap forming a common cloud of ions within the cluster's area. The number density of ions

within a dust cluster is much greater than that in unperturbed, isotropic plasma.

The stable 2D dust cluster is a unique system to investigate the influence of an ion flow on the plasma structure and the charge on grains. The ion drift induces an anisotropy affecting the non-linear charging and screening of grains, the distributions of ions and electrons, electric potential and charge density. The common potential well deforms transforming to a shallow oval basin with formation of an elongated potential hill behind the dust cluster. Our PIC results reveal that the wake with strong ion focusing is developed when the ion flow is supersonic. This common wakefield is formed due to a collective contribution of cluster's grains. The number density of ions in the common ion cloud significantly exceeds that in the bulk plasma and within a cluster. The area within a dust cluster remains highly depleted of electrons even at supersonic ion flows. However, strips of electron density are formed in the region of the ion focus behind a cluster presumably maintaining the quasineutrality of the plasma space charge.

The supersonic ion flow modifies the distribution of the charge density on and around grains in a cluster. It is shown that the charge on grain 2 becomes positive meaning that the electrostatic attraction between this positively charged grain and nearby negatively charged grains can be established. Thus, a new type of interaction between grains can arise within a dust cluster. This phenomenon is due to a drastic change in the plasma structure within a dust cluster. We presume that the positive charge on grain 2 is due to the ion focusing behind the first grain in the central row.

The laser heating, neutral gas flow and ion wakefield attraction can be used to excite 2D finite dust clusters causing their oscillations and rearrangements. The stability of a 2D dust cluster can also be affected by variations in the ion flow speed. The kinetic-level PIC results provide insights into the development of instabilities that initiate the cluster melting. Indeed, the formation of the ion wake focus with the change in the plasma structure, such as redistribution of ions and electrons, imposes the force on dust grains leading to their rearrangement, transition to other ordering configuration or disordering. However, these grain rearrangements occurring during milliseconds and seconds are beyond timescales of our PIC modeling.

Acknowledgments

This work is supported by the US Department of Energy, Office of Fusion Energy Sciences. TeraGrid computational resources provided by the NCSA under grant TG-PHY090096.

References

- [1] Ignatov A M 2005 *Plasma Phys. Rep.* **31** 46
- [2] Ishihara O 2007 *J. Phys. D: Appl. Phys.* **40** R121
- [3] Bonitz M, Henning C and Block D 2010 *Rep. Prog. Phys.* **73** 066501
- [4] Ikezi H 1986 *Phys. Fluids* **29** 1764
- [5] Chu H and Lin I 1994 *Phys. Rev. Lett.* **72** 4009
- [6] Thomas H, Morfill G E, Demmel V, Goree J, Feuerbacher B and Mohlmann D 1994 *Phys. Rev. Lett.* **73** 652
- [7] Hayashi Y and Tachibana K 1994 *Japan. J. Appl. Phys.* **33** L804
- [8] Juan W-T, Huang Z-H, Hsu J-W, Lai Y-J and Lin I 1998 *Phys. Rev. E* **58** 6947
- [9] Arp O, Block D, Piel A and Melzer A 2004 *Phys. Rev. Lett.* **93** 165004
- [10] Usachev A D, Zobnin A V, Petrov O F, Fortov V E, Annaratone B M, Thoma M H, Hfner H, Kretschmer M, Fink M and Morfill G E 2009 *Phys. Rev. Lett.* **102** 045001
- [11] Hug J E, van Swol F and Zukoski C F 1995 *Langmuir* **11** 111
- [12] Naser S, Palberg T, Blechinger C and Leiderer P 1997 *Prog. Colloid Polym. Sci.* **104** 194
- [13] Leiderer P, Ebner W and Shikin V B 1987 *Surf. Sci.* **113** 405
- [14] Vladimirov S V and Samarian A A 2007 *Plasma Phys. Control. Fusion* **49** B95
- [15] Melzer A, Buttenschon B, Miksch T, Passvogel M, Block D, Arp O and Piel A 2010 *Plasma Phys. Control. Fusion* **52** 124028
- [16] Lai Y-J and Lin I 1999 *Phys. Rev. E* **60** 4743
- [17] Davoudabadi M and Mashayek F 2007 *Phys. Rev. E* **76** 056405
- [18] Schweigert V A and Peeters F 1995 *Phys. Rev. B* **51** 7700
- [19] Melzer A, Klindworth M and Piel A 2001 *Phys. Rev. Lett.* **87** 115002
- [20] Melzer A 2003 *Phys. Rev. E* **67** 016411
- [21] Barkby S, Vladimirov S V and Samarian A A 2008 *Phys. Lett. A* **372** 1501
- [22] Wolter M and Melzer A 2005 *Phys. Rev. E* **71** 036414
- [23] Ichiki R, Ivanov Y, Wolter M, Kawai Y and Melzer A 2004 *Phys. Rev. E* **70** 066404
- [24] Ivanov Y and Melzer A 2005 *Phys. Plasmas* **12** 072110
- [25] Melzer A 2006 *Phys. Rev. E* **73** 056404
- [26] Klindworth M, Melzer A and Piel A 2000 *Phys. Rev. B* **61** 8404
- [27] Tsytoich V N, Morfill G E, Vladimirov S V and Thomas H M 2008 *Elementary Physics of Complex Plasmas (Lecture Notes in Physics vol 731)* (Berlin: Springer)
- [28] Shukla K and Mamun A A 2002 *Introduction to Dusty Plasma Physics* (Bristol: Institute of Physics) chapter 8
- [29] Nambu M, Vladimirov S V and Shukla P K 1995 *Phys. Lett. A* **203** 40
- [30] Shukla P K and Rao N N 1996 *Phys. Plasmas* **3** 1770
- [31] Shukla P K and Eliasson B 2009 *Rev. Mod. Phys.* **81** 25
- [32] Maierov S A, Vladimirov S V and Cramer N F 2001 *Phys. Rev. E* **63** 017401
- [33] Vladimirov S V, Maierov S A and Cramer N F 2003 *Phys. Rev. E* **67** 016407
- [34] Vladimirov S V, Maierov S A and Ishihara O 2003 *Phys. Plasmas* **10** 3867
- [35] Samarian A A and Vladimirov S V 2009 *Contrib. Plasma Phys.* **49** 260
- [36] Miloch W J, Trulsen J and Pécseli H L 2008 *Phys. Rev. E* **77** 056408
- [37] Miloch W J 2010 *Plasma Phys. Control. Fusion* **52** 124004
- [38] Miloch W J, Kroll M and Block D 2010 *Phys. Plasmas* **17** 103703
- [39] Hockney R W and Eastwood J W 1981 *Computer Simulation Using Particles* (New York: McGraw-Hill)
- [40] Birdsall C K and Langdon A B 1985 *Plasma Physics via Computer Simulation* (New York: McGraw-Hill)
- [41] Joyce G, Lampe M and Ganguli G 2002 *Particle simulation of dusty plasmas Space Plasma Simulations vol 615* (Heidelberg: Springer)
- [42] Matyash K, Schneider R, Taccogna F and Tskhakaya D 2007 *J. Nucl. Mater.* **363–365** 458
- [43] Matyash K, Schneider R, Ikkurthi R, Lewerentz L and Melzer A 2010 *Plasma Phys. Control. Fusion* **52** 124016
- [44] Amestoy P R, Guermouche A, L'Excellent J Y and Pralet S 2006 *Parallel Comput.* **32** 136

- [45] Miloch W J, Pécseli H L and Trulsen J 2007 *Nonlinear Process. Geophys.* **14** 575
- [46] Miloshevsky G V and Hassanein A 2012 *Phys. Rev. E*, submitted
- [47] Tsytovich V N, Khodataev Ya K and Bingham R 1996 *Comment. Plasma Phys. Control. Fusion* **17** 249
- [48] Resendes D P, Mendonga J T and Shukla P K 1998 *Phys. Lett. A* **239** 181
- [49] Ivanov A S 2001 *Phys. Lett. A* **290** 304
- [50] Khodataev Ya, Bingham R, Tarakanov V, Tsytovich V and Morfill G 2001 *Phys. Scr.* **T89** 95
- [51] Tsytovich V N, Gousein-zade N G and Morfill G E 2006 *Phys. Plasmas* **13** 033503
- [52] Rovagnati B, Davoudabadi M, Mashayek F and Lapenta G 2007 *J. Appl. Phys.* **102** 073302
- [53] Shukla P K 2011 Experiments and theory of dusty plasmas *Dusty/Complex Plasmas: Basic and Interdisciplinary Research* ed N Yu Nosenko *AIP Conf. Proc.* **1397** 11
- [54] Morfill G E, Annaratone B M, Bryant P M, Ivlev A V, Thomas H M, Zuzic M and Fortov V E 2002 *Plasma Phys. Control. Fusion* **44** B263
- [55] Maierov S A 2005 *Plasma Phys. Rep.* **31** 690